Analysis of the mesoscale structure in the IMECOCAL region (off Baja California) from hydrographic, ADCP and altimetry data

Luis Soto-Mardones[a,b,*], Alejandro Parés-Sierra[c], Joaquín Garcia[c], Reginaldo Durazo[b], Samuel Hormazabal[d]

[a]*Universidad del Bio-Bio, Concepción, Chile*
[b]*Universidad Autónoma de Baja California, Ensenada, México*
[c]*Centro de Investigación Científica y de Educación Superior de Ensenada, Ensenada, México*
[d]*Danish Center for Earth System Science, Niels Bohr Institute for Astronomy, Physics and Geophysics, University of Copenhagen, DK-2100 Copenhagen, Denmark*

Abstract

We present geostrophic velocities obtained using hydrographic-altimeter data and direct measurements of currents from 11 cruises offshore of Baja California from January 2000 to July 2002. The study area was dominated by meanders and eddies in geostrophic balance. Two mechanisms of eddy generation were observed; the first associated with the geometry of the coastline, and the second a product of the cooling of the California Current and the California Undercurrent from the South. There were two persistent eddies observed during the study. The first eddy was offshore of Bahía Vizcaíno and had an anticyclonic circulation. Situated in the southern region, the rotation of the second eddy was dependant on which current was first to enter the transition zone along the coast. Spring was a transition period characterized by the formation of meanders. The summer brought a period of eddy generation along the coast. Autumn and winter were marked by a separation of eddies from the coast and their subsequent drift towards the west. The phase velocity of the mesoscale eddies was in accordance with the theory of the linear propagation of a Rossby wave.
© 2004 Published by Elsevier Ltd.

1. Introduction

The California Current System (CCS) is a dynamic system influenced by a large anticyclonic eddy in the Northern Hemisphere (Hickey, 1979; Halliwell et al., 1983) and an area of low pressure over North America (Pond and Pickard, 1978).

*Corresponding author. Universidad del Bio-Bio, Concepción, Chile.

E-mail address: lsoto@cicese.mx (L. Soto-Mardones).

The surface circulation of the CCS has been described by various authors such as Hickey (1979), Chelton (1982) and Lynn and Simpson (1987). The CCS in the study region includes the California Current (CC), which flows at the surface towards the Equator, and the California Undercurrent (CUC), which has a subsurface flow towards the pole along the coasts of Baja California and Southern California. During the usual periods of upwelling between April and September, the CC completely covers the CUC.

It has been show that eddies and meander are complex dynamic structures that greatly influence biological process. For examples Aguirre-Hernandez et al. (2004), show that for the same Investigaciones Mexicanas de la Corriente de California (IMECOCAL) region the most dynamicaly actives region (i.e. N, E) coincides with the most productive area. The dynamic processes responsible for the generation and evolution of the complex structures of meanders, eddies and filaments in the CCS were studied by Strub et al. (1991). Possible mechanisms that generate these complex structures include barotropic and baroclinic instabilities of the coastal flow, wind-driven Ekman transport, intense upwelling and irregular coastline, among others (see Gill, 1982). These generating mechanisms have been explored by several authors using numerical modeling, such as Ikeda and Emery (1984), Ikeda et al. (1984a, b) and Haidvogel et al. (1991). Ikeda et al. (1984a) suggested that baroclinic instabilities play an important role in the generation of meanders. Haidvogel et al. (1991) showed that the development of the instabilities is a product of the combination of a coastal jet with an equatorward flow, the bottom topography and the highly irregular coastline.

Another possible generating mechanism of the mesoscale variations in the CCS is wind forcing which acts upon the coastal current to produce instabilities that can lead to the formation meanders, eddies, and filaments. These mechanisms have been explored by Batteen et al. (1989), Auad et al. (1991), McCreary et al. (1992), Parés-Sierra et al. (1993) and Batteen (1997). Using satellite data, Strub and James (2000) defined a conceptual scheme for the seasonal evolution of the circula-tion of the CCS. Strub and James (2000) proposed that in spring and summer, an equatorward flow develops close to shore with an initial meridional structure that responds to the equatorward winds blowing along the shore. The mechanisms that create this seasonal flow are associated with local upwelling fronts that are displaced offshore of the shelf by the oceanic offshore flow. This flow moves towards the west until approximately 130°W where it is weakened and dissipates in autumn and spring. Strub and James (2000) do not explain the dynamics that control the westward flow or its dissipation, but the velocity of the westward flow is consistent with Rossby wave dynamics.

Using hydrographic data, direct current measurements and sea-level anomalies, we present the seasonal circulation of the region of Baja California, México, showing the eddy formation and its westward drift from these three independent measurements.

2. Data and methods

Fig. 1 shows the distribution of the hydrographic stations during the project IMECOCAL, a subset of the original California Cooperative Fisheries Investigations (CalCOFI) program. The distance between stations was 37 km and the distance between transects was 74 km. Temperature, salinity and current data (Acoustic Doppler current Profiler, ADCP) were registered and calibrated in the Laboratorio de Oceanografía Regional del Centro de Investigación Científica y de Educación Superior de Ensenada (CICESE). The calibration of the (Conductivity Temperature and Depth) CTD and preliminary processing of the data are described by García et al. (1999). The data from the 11 cruises used in this study cover the period from January 2000 to August 2002 (Table 1).

At each station, conductivity, temperature and pressure (CTD) were sampled to a minimum depth of 1000 m using a Seabird CTD armed with primary and secondary temperature and conductivity sensors. Temperature and conductivity sensors were factory-calibrated prior to each cruise and sensor drift between calibrations was observed

to be less than expected (<0.003°C and <0.006 mmho cm^{-1} for temperature and conductivity, respectively).
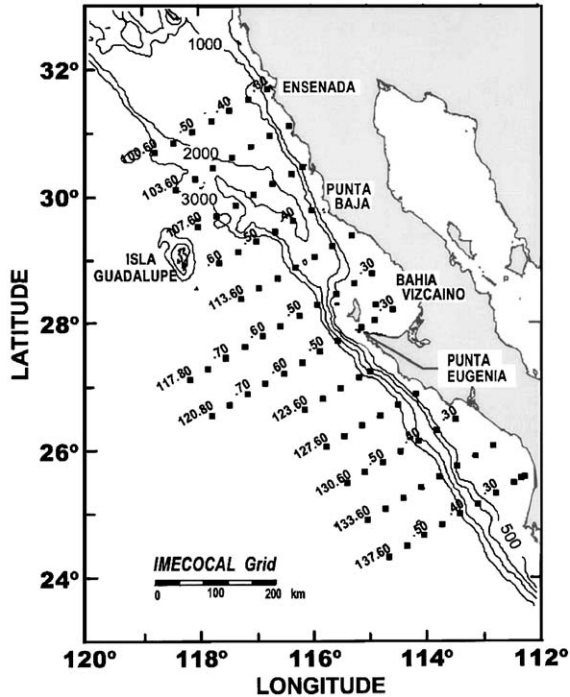
Fig. 1. Map of the study area showing subset of the original CalCOFI grid covered by the IMECOCAL surveys. Solid circles indicate station positions. Depth contours are in meters.

Velocity profiles along the ship track were obtained with an RD Instruments hull-mounted 153.6 kHz broad-band Acoustic Doppler Current Profiler (ADCP-BBVM). Measurement ensembles were obtained every 11 s using a pulse length of 8 m and a vertical size of 8 m. Typical depth ranged from 0 to 300 m, with the most reliable data found between 20 and 180 m. For the results presented herein, the shortest time-averaging interval used is 3 and 5 min for the 0204, for which the inherent random uncertainty in the average ADCP velocity was ± 0.01 and ± 0.008 ms^{-1} respectively. Bottom tracking was used to obtain ship velocity, (± 0.01 ms^{-1}) when the bottom was visible to the ADCP. In deep water, global positioning system (GPS) navigation was used to calculate ship velocity, and this was then smoothed using a Blackman window of width $T = 30$ min (Firing et al., 1995). For each cruise, a calibration run on the heading data was made to eliminate any rotation of the ADCP relative to the gyrocompass (Firing et al., 1995). The uncertainty due to navigation is ± 0.04 ms^{-1}. In summary, when bottom tracking is available, overall error in 3 and 5 min averaged absolute ADCP velocity is estimated to be ± 0.02 and ± 0.018 ms^{-1}, respectively. When bottom tracking is not available (i.e. ocean depths greater than 400 m), the absolute velocity has a random uncertainty due to navigation of ± 0.05 ms^{-1}.

Covering the area 130°W–113°W and 24°N–32°N, maps of sea-level anomalies (SLA)

Table 1
Name, dates and number of stations taken during the cruises off Baja California for the IMECOCAL program

Cruise name	Dates	Number of stations	ADCP	SLA
'0001'	01/14/2000–01/31/2000	90		X
'0004'	04/04/2000–04/22/2000	73		X
'0007'	07/11/2000–07/30/2000	82		X
'0010'	10/10/2000–10/29/2000	88	x	X
'0101'	01/16/2001–02/03/2001	73	x	X
'0104'	04/07/2001–04/12/2001	17	x	X
'0106'	06/26/2001–07/15/2001	83	x	X
'0110'	10/04/2001–10/23/2001	90	x	
'0201'	01/19/2002–02/05/2002	72	x	
'0204'	04/19/2002–05/07/2002	72	x	
'0207'	07/12/2002–08/02/2002	91		

Cruises were conducted on the B.O. *Francisco de Ulloa*. Column 4 shows the periods in which measurements of ADCP were made and column 5 shows the periods that include altimetry data.

were obtained from the TOPEX/Poseidon (T/P) instrument and the ERS 1–2 Satellite Scatterometer (http://www-aviso.cnes.fr:8090). The temporal sequence was every 10 days with a spatial grid $0.25° × 0.25°$. The available data only covers the period from January 2000 to August 2001 (see Table 1). For more information on the altimetric corrections applied in the T/P and ERS 1–2 SSH missions, refer to Le Traon and Ogor (1998). The methodology used to obtain the geostrophic anomalies was that proposed by Ducet and Le Traon (2000).

Using hydrographic data and SLA, surface fields of the geostrophic flows were referenced to 500 dbar. This reference level was chosen in order to be comparable to historic results from CAL-COFI and IMECOCAL.

Wind fields were obtained from the QuikSCAT mission (http://winds.jpl.nasa.gov/). The temporal resolution was daily, and the spatial resolution was $0.5° × 0.5°$. From the wind fields, spatial maps were created for the period of each cruise. Using these maps, the Ekman drift was calculated using the method proposed by Madsen (1997).

3. Analysis and results

For the year 2000, Fig. 2 shows the maps of sea-surface dynamic height with respect to 500 dbar (solid lines) and the geostrophic velocities (black arrows) calculated using hydrographic data. During spring and summer (Figs. 2B and C), a strong southward flowing CC can be seen and this is consistent with observations in the climatology by Lynn and Simpson (1987). In fall, the flow persists towards the Equator, but along the coast the direct ADCP measurements show the presence of a surface counter current up to Punta Eugenia. This surface counter current has been described by various authors such as Roden (1971), Lynn and Simpson (1987), and Durazo and Baumgartner (2002).

In winter (Fig. 2A), various eddies are observed in the region: a cyclonic eddy at ∼30.7°N, an anticyclonic eddy in front of Bahía Vizcaíno at ∼28.2°N, and another weak cyclonic eddy at ∼26.5°N. In spring, the circulation is more homogeneous with no distinctive eddy formation (Fig. 2B), although a considerable meander is shown in front of Bahía Vizcaíno, which appears to be the initial stage of a new eddy. The increase of the coastal equatorward current in the southern region (between 27°N and 25°N) is associated with the presence of an anticiclonic eddy in the region. Due to the limits of the grid, it is not possible to determine if the eddy that forms in winter is propagating towards the ocean, as is observed in Isla Guadalupe (Fig. 2B). This possibility will be explored later with the SLA. In summer (Fig. 2C), the eddies form in front of San Quintín (cyclonic eddy), off Isla Guadalupe (anticyclonic eddy) and in front of Punta Eugenia (cyclonic eddy). Lastly, in fall (Fig. 2D), we observe two eddies with opposite rotation: an anticyclonic eddy in front of Bahía Vizcaíno (∼28.8°N, 116°W) and a cyclonic eddy in front of Punta Eugenia. For the southern region, the circulations directly obtained by the ADCP are very similar to those obtained by geostrophic calculations.

The expeditions in 2001 were characterized by the complete incorporation of ADCP measurements. In winter (Fig. 3A) in the oceanic zone (∼30°N and 28°N), two anticyclonically rotating eddies were observed, apparently generated by the separation of meanders. This observation (i.e. existence of two anticyclonic eddies) is corroborated by the SLA images and direct ADCP observations (as shown in the next section) and by the circulation calculated from hydrographic data. These independent data sources also confirm the existence of a smaller cyclonic eddy closer to the coast in front of San Quintin (∼30°N), which can be seen in greater detail. In spring (Fig. 3B), the only available data is the ADCP and this exists only for the northern region (∼28°–32°N). However, given the high coherence shown between ADCP and geostrophic data in the previous cruises, we can describe the typical circulation for this period as a formation of meanders in the northern region. In summer near the coast (Fig. 3c), cyclonic eddies are seen in the northern (∼30°N, −116.5°W), central (∼28°N, −115.7°W) and southern (∼26°N) regions. The similarity between the direct ADCP measurements and the geostrophic velocities is evident. In autumn in the
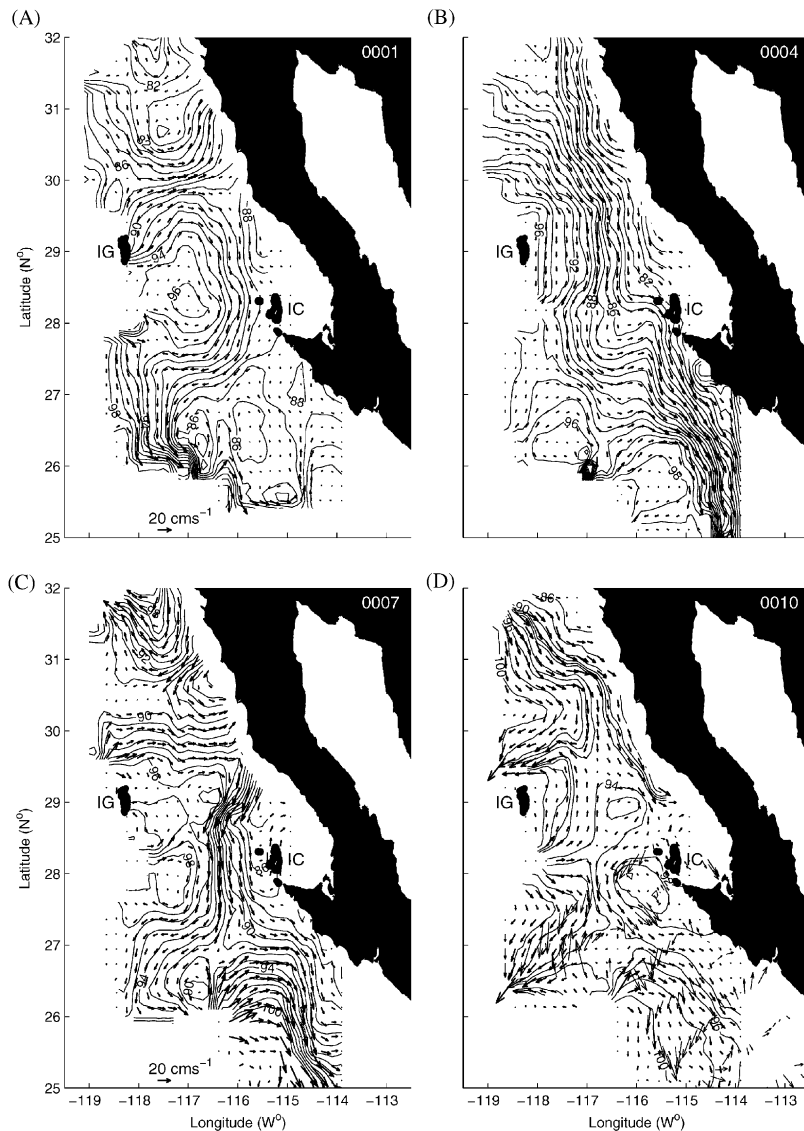
Fig. 2. Maps of dynamic heights (in dynamic meters) relative to 500 dbar (solid contour) and associated geostrophic velocity in cm s^{-1} (arrows). For 2000, the cruises are: (A) January, (B) April, (C) July, and (D) October. The October cruise includes direct velocity observations from shipboard (cm s^{-1}).

northern region (Fig. 3D), there is a separation of the cyclonic eddy ($\sim$30.5°N), which intensifies the flow on the west side. Towards the southern region, a small cyclonically rotating eddy ($\sim$26.8°N) is visible. Again, the ADCP measurements agree with the geostrophic circulation as far as the central region.

During the winter of 2002 (Fig. 4A), there is a southward flow with pronounced meanders. There are two large eddies that circulate in opposite directions: one in the central region ($\sim$29°N) that rotates in an anticyclonic direction with diameter of approximately 120 km, and a second smaller eddy rotating cyclonically in front of Punta
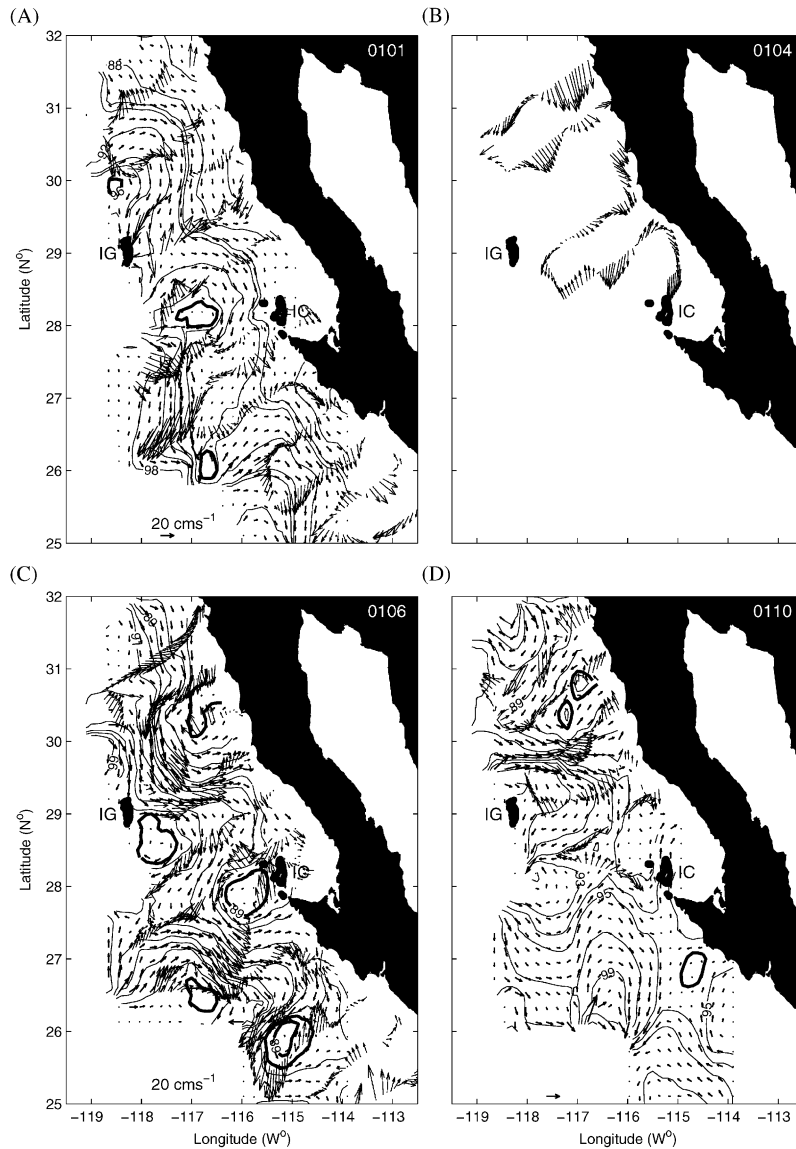
Fig. 3. Maps of dynamic heights (in dynamic meters) relative to 500/0 dbar (solid contour) and associated geotrophic velocity in cm s^{-1} (arrows). For 2001, the available cruises are (A) January, (B) April, (C) August, and (D) October. All the cruises include direct velocity observations from shipboard (cm s^{-1}). The April cruise does not include measurement of dynamic heights.

Eugenia. The ADCP measurements again show coherence with geostrophic velocities. In spring (Fig. 4B), continuous circulation continues towards the south, with smooth meanders and no eddies formed along the coast. However, during the summer, the formation of eddies clearly appears along the entire study region (Fig. 4C).

The two independent measurements used in this study (i.e. geostrophic velocities and ADCP) show good qualitative correlation. We can infer that the surface circulation in the area during spring occurs towards the south with smooth meanders that follow the coast-line (Figs. 2B, 3B and 4B). There is also an intensification of the current to the south
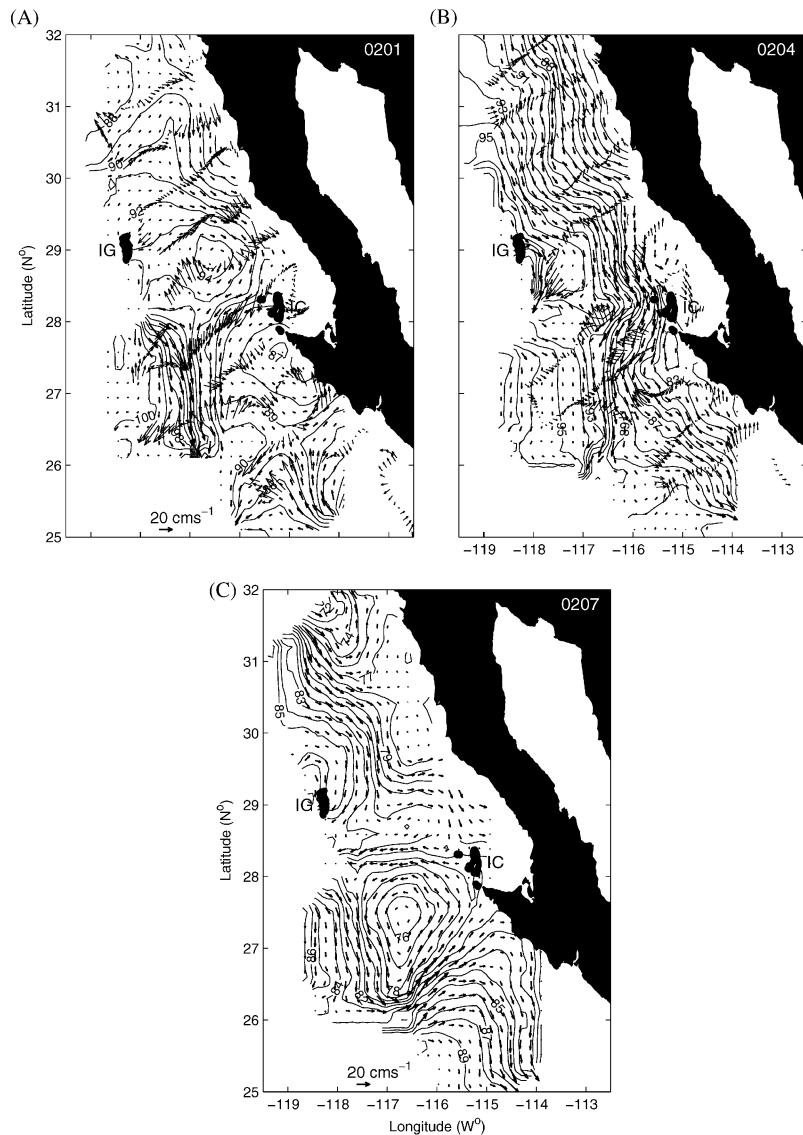
Fig. 4. Maps of dynamic heights (in dynamic meters) relative to 500/0 dbar (solid contour) and associated geostrophic velocity in cm s^{-1} (arrows). For 2002, the available cruises are: (A) January, (B) April, and (C) July. The cruises in January and April include direct velocity observations from shipboard (cm s^{-1}).

of our study area. This characteristic of the coastal current has been observed by Lynn and Simpson (1987). The summer is characterized by the appearance of small eddies in the region close to shore that interact with the CC. For example, the background current increases the circulation on the eastern side of anticyclonic eddies while reducing their western side. Similarly, a cyclonic eddy would experience the inverse effect. In autumn, the eddies are completely formed and begin to separate from the coast and move towards the open ocean. Finally, in winter, the eddies drift towards the west to interact with the coastal ocean. Most of the observed eddies in front of Bahía Vizcaíno (e.g., around 28.5°N, 117°W in Figs. 2A, 2C and D) are anticyclonic, suggesting
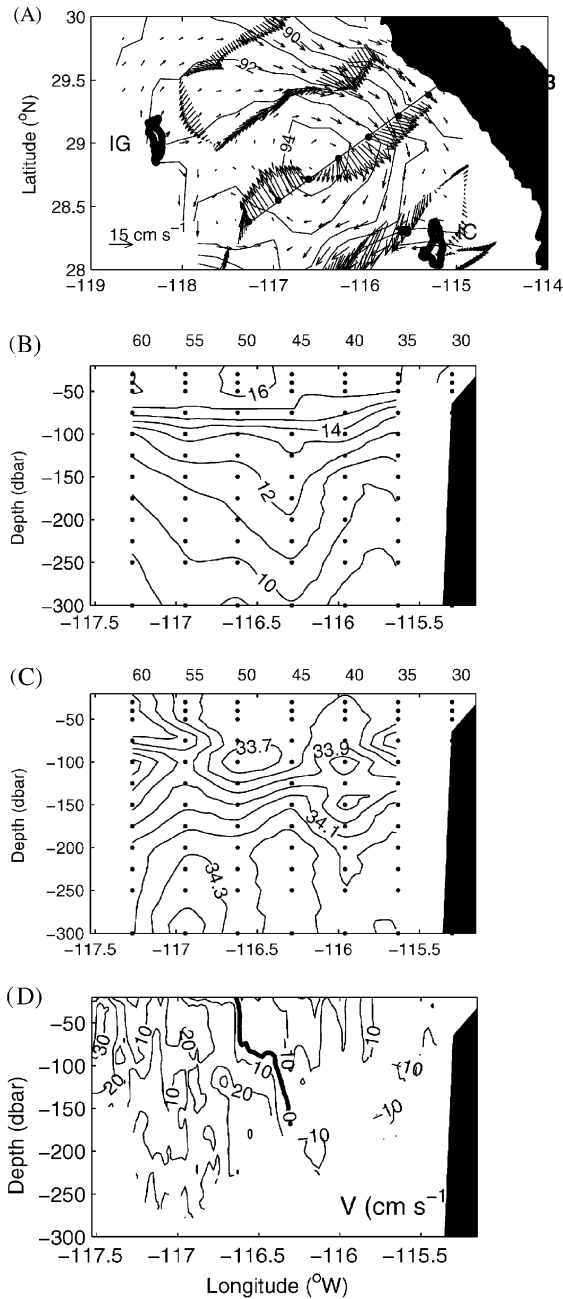
Fig. 5. An anticyclonic gyre is present in January 2001. (A) Maps of dynamics height (in dynamic meters) at the sea surface relative to 500 dbar (solid contour), with its respective geostrophic velocity (arrows) and direct velocity observations from shipboard. In line 113, are the vertical distributions of (B) temperature (°C), (C) salinity, and (D) direct velocity observations.
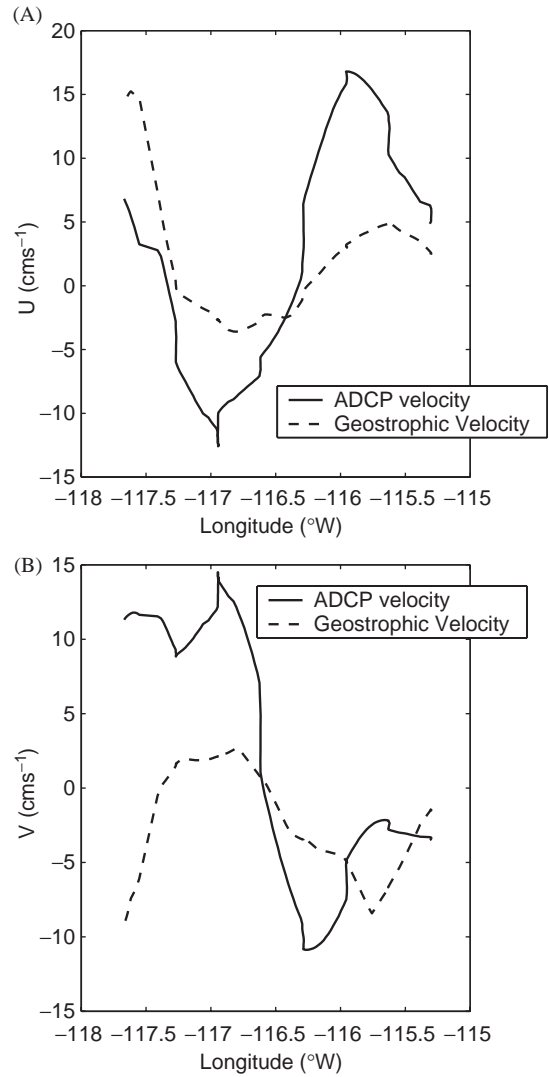
Fig. 6. Geostrophic and ADCP velocities along the 113 line for: (A) East-west component and (B) north–south component.

that the CC is causing these eddies to take the form of the bay near the latitude of Ensenada (31°N) where the CC becomes more coastal. The eddies formed in front of Punta Eugenia are mainly cyclonic and generally result (e.g., Figs. 2D, 3C, 4A and 4C) from the influence of Punta Eugenia and the surface counter current flowing from the south. Though the counter current remains present, this process does not occur during the spring, as indicated by the ADCP measure-

(A)

(B)
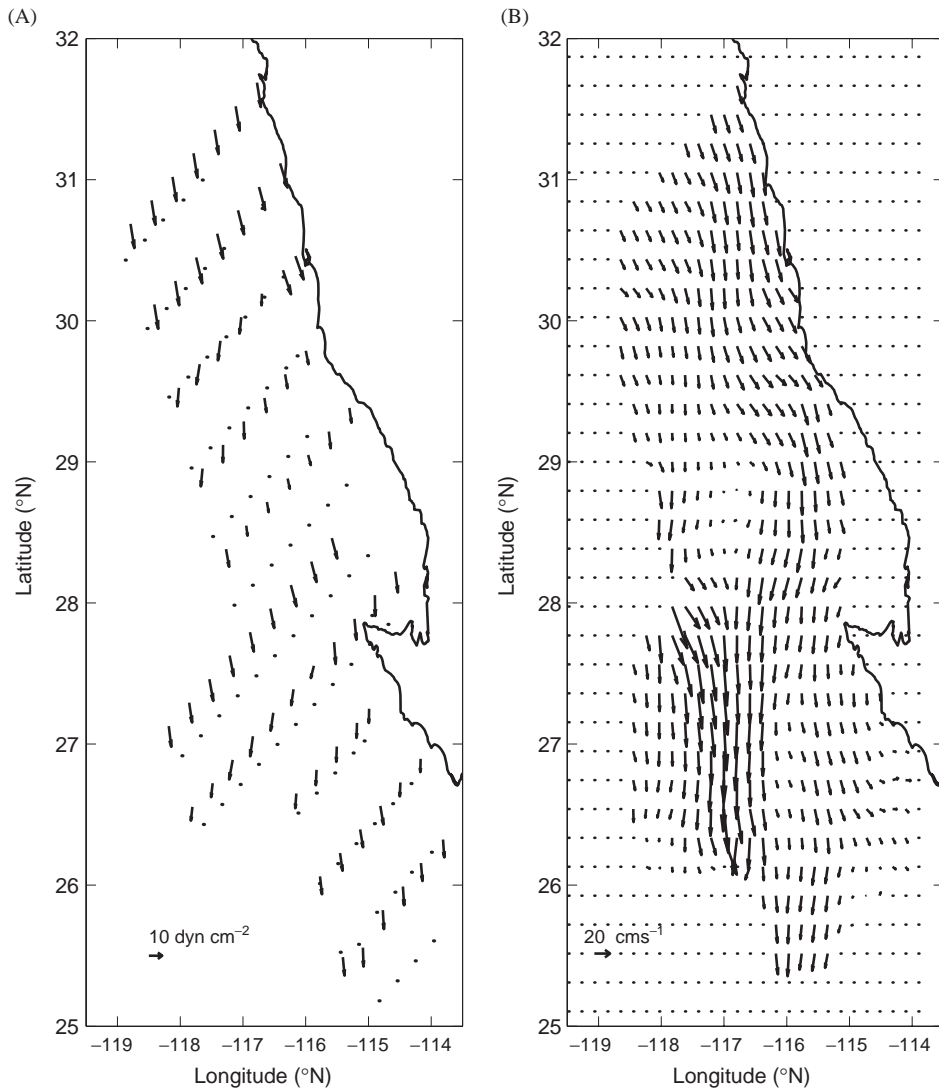
Fig. 7. Surface distribution of the January 2001 QuikSCAT wind stress (dyn cm^{-2}) (A) and Ekman transport (cm s^{-1}) (B).

ments (Fig. 4C) along the coast (between 25°N and 28°N).

In order to observe the spatial structure of the eddies, we can consider a particular case during the winter of 2002; an anticyclonic eddy offshore of Bahía Vizcaíno (Fig. 5A) with a center of rotation focused on line 113 and an approximate diameter of 200 km. Again, we note the similarity between ADCP and geostrophic velocities. As

indicated by the vertical distribution of temperature (Fig. 5B), the vertical extent of the eddy is greater than 300 m. The salinity minimum coincides with the center of both the eddy and the CC (Fig. 5C). Measured with the ADCP, the vertical distribution of current velocities perpendicular to the transect (Fig. 5D) agrees with the hydrographic structure of the eddy and its vertical extent of ~350 m. The ADCP data and the tilted
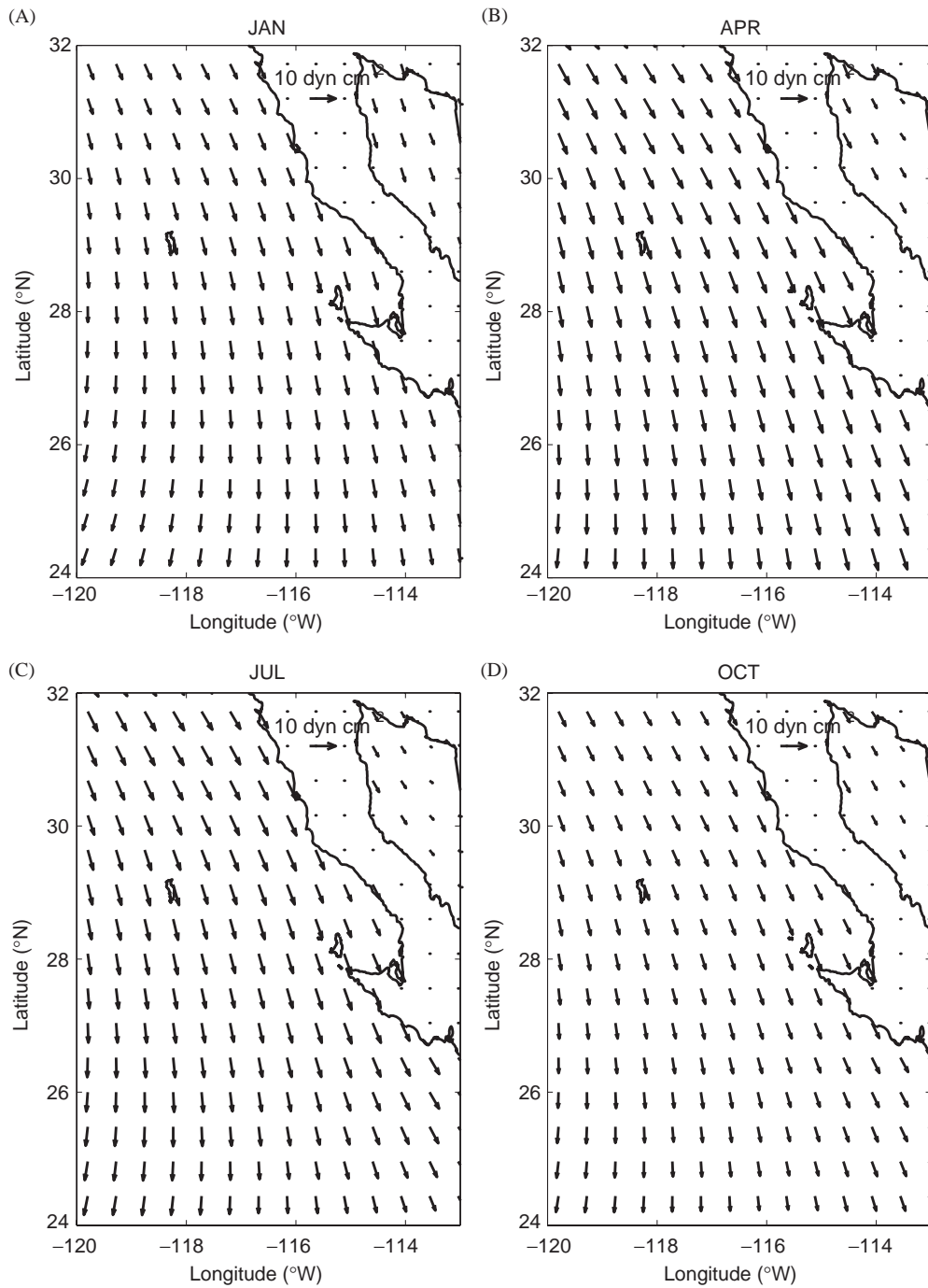
Fig. 8. Climatology of the wind stress (September 1998 to Sepatember 2002) for (A) January, (B) April, (C) July, abd (D) August.
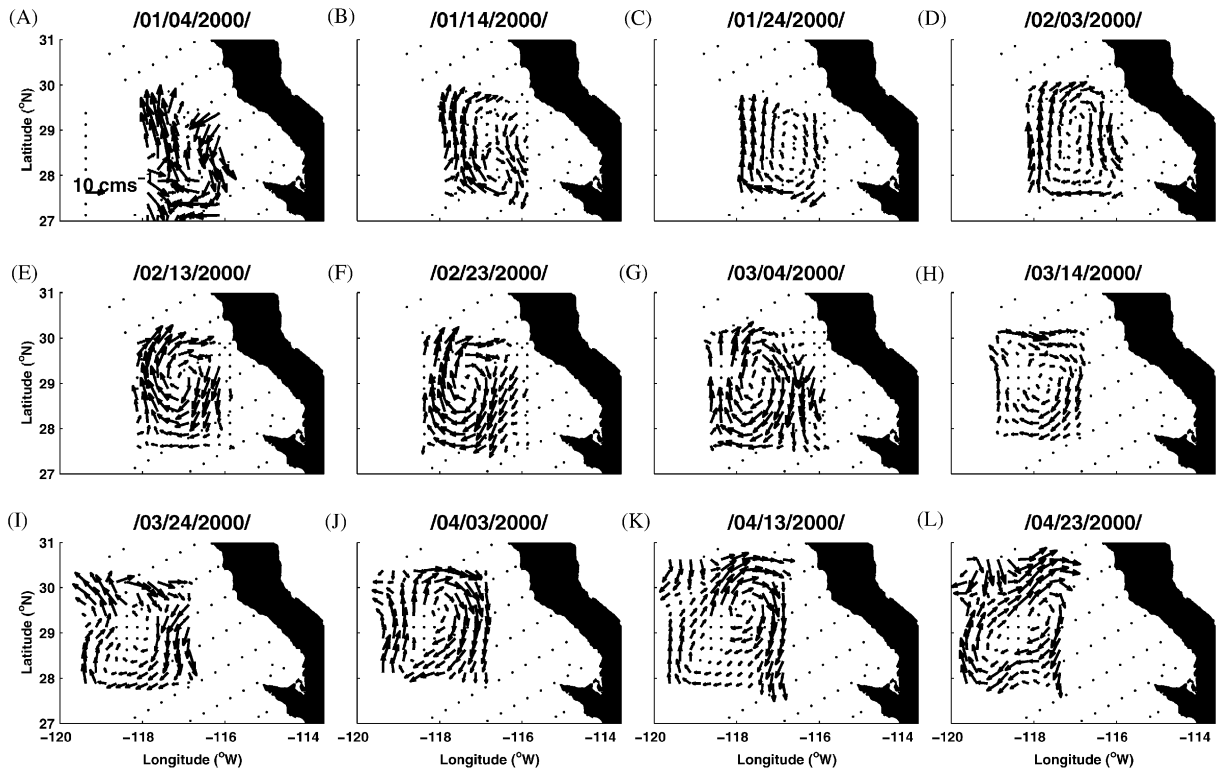
Fig. 9. Maps of geostrp[hic velocities calculated from altimetry data (i.e., TOPEX and ERS1-2). The time sequence corresponds to 10 days intervals and a $0.25 \times 0.25°$ spatial resolution.

isotherms (Fig. 5B) show that the deep end of the eddy core has shifted inshore which suggests that the eddy is moving offshore.

The similarities observed between the geostrophic circulation and the absolute velocities measured with the ADCP validate the results obtained from hydrographic data and indicate that the circulation in the region is mostly geostrophic. However, there are some differences in the magnitude of the velocity fields that are most likely associated with the non-geostrophic components. The ADCP measures total current, including non-geostrophic components such as Ekman drift, tides and near-inertial motions. Figs. 6A and B show the structure of horizontal velocities (U and V) obtained for line 113. Current directions are the same in both figures but the magnitudes are much smaller for geostrophic currents. A number of authors have dealt with these differences using model-fitting techniques (Chereskin et al., 1989;

Candela et al., 1992) or through a grinding technique that forces geostrophic balance (Bretherton et al., 1976; Walstad et al., 1991; Chereskin and Trunnell, 1996). In our case, as a first approximation, we computed Ekman drift from QuikSCAT winds for all cruises. An example is shown in Fig. 7, with the wind stress computed for cruise 0201. We interpolated these winds and generated a grid similar to that used for the geostrophic calculations.

The Ekman transport was calculated for this new grid using the methods described by Madsen (1977). Fig. 7B shows the transport obtained by adding the Ekman transport to the calculation using geostrophy as shown in Fig. 4A. It is evident that the Ekman transport increases the equatorward transport and changes the structure of eddies and meanders, reinforcing the circulation in the eastern part of the anticyclonic eddies and the western half of the cyclonic eddies. Similar
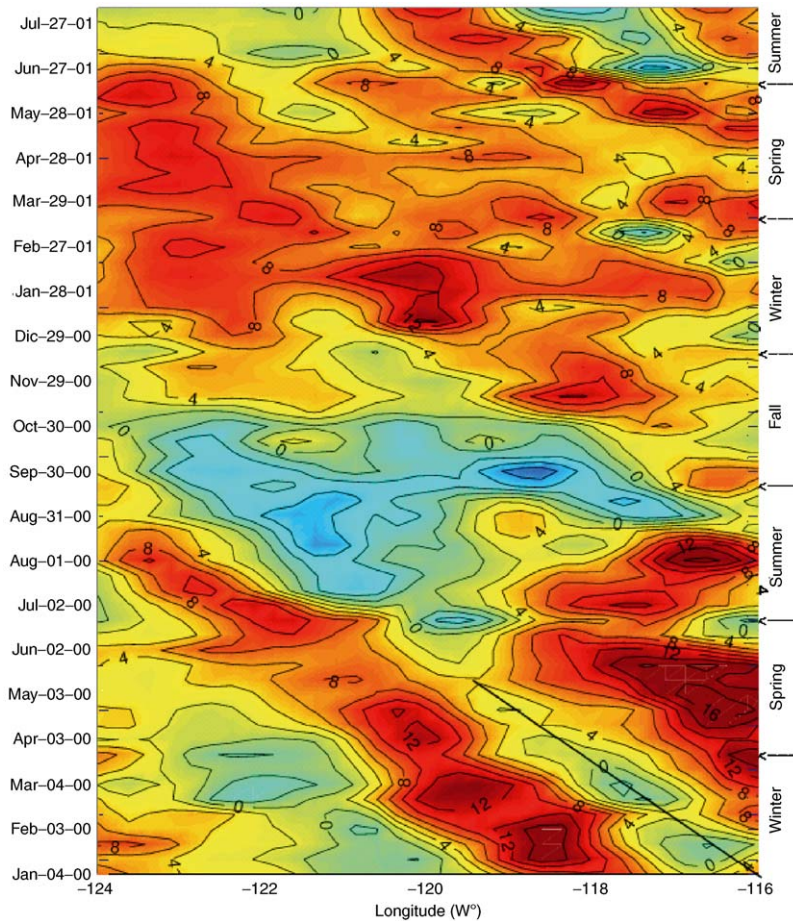
Fig. 10. Hovmüller diagrams for sea-level height from altimetry at 28.5°N. Contour lines are every 4 cm. Dark lines mark the presence of anticyclonic eddies (i.e. positive height anomalies) its slope indicates a propagation speed of approximately 0.04 cm s^{-1}.

calculations were performed for the 1999 period by Figueroa (2002) who reports the same behavior. The objective of this work is not to explain the differences in amplitude, but to demonstrate the existence of mesoscale eddies for the area by means of independent techniques.

Computed from three years of data spanning September 1999 to 2002, the annual cycle of the wind stress is shown in Fig. 8. The wind is considerable compared to the seasonal variability for the majority of the year when the winds are southeastward, parallel to the coastline and favoring upwelling. Away from the coast, near Guadalupe Island, the winds tend to shift slightly toward the south. The wind stress is stronger

during the spring and summer seasons (Figs. 8B and C), but it is more uniform in magnitude and direction during spring. In fall and winter (Figs. 6D and A), the winds are weaker along the coast.

Due to the poor longitudinal sampling coverage (~3°W), it was not possible to follow the observed eddies in the horizontal maps (Figs. 2–4). From altimetry sea level data, geostrophic velocities were calculated using the methodology proposed by Ducet and Le Traon (2000). With these surface maps, it is possible to follow the displacement of the anticyclonic eddy initially positioned at Bahía Vizcaíno. This eddy is also evident in the hydrographic data and in the directly measured velocity ADCP velocities (Fig. 2A). The image sequence

shown in Fig. 9 represents snapshots with ten-days intervals. Figs. 9B–D, coincide with cruise 0001 and Figs. 9J–I coincide with cruise 0 0 2. The westward propagation of this eddy is clearly evident in Fig. 9.

In order to determine the propagation velocity of the eddies, a Hovmüller diagram was computed from zonal transect of the altimetry SSH data at Bahía Vizcaíno (at approximately 28.5°N, Fig. 10). This has been determined to be an area of generation of anticyclonic eddies (Lynn and Simpson, 1987, and Durazo and Baumgartner, 2002). In Fig. 10, positive anomalies are associated with an elevation of the surface and eddies that rotate anticyclonically. The 118°W–116°W band defines an area where the mesoscale eddies are more evident. They form and propagate through-out the entire year, even though there is no clear seasonal periodicity in their generation. The eddy shown in Fig. 9 lasts for approximately 7 months and has a propagation velocity of approximately $0.04\,\text{m s}^{-1}$. In general, the propagation slope is similar for all the eddies and compares well to Rossby wave linear theory (see Fig. 10). The theoretical propagating speed of a free Rossby wave was computed using a linearly interpolated upper layer depth (H) from 150 m at 30°N to 300 m at 22°N (e.g., White and Saur, 1983, Pares-Sierra and O'Brien, 1989, Herrera and Pares-Sierra, 1994). With this depth, and a reduced gravity of $0.04\,\text{m s}^{-1}$, the propagation phase speed was calculated using the formula

$$c = \beta(g'H)/f^2, \tag{1}$$

where β is the variation of the Coriolis parameter with latitude. Using (1) and the parameters mentioned above, the phase speed for a Rossby wave at 28.5°N is found to be $0.024\,\text{m s}^{-1}$. The Rossby wave speed in (1) is a long-wave result so that it is independent of wavelength.

4. Conclusions

The analyses of the three independent variables of hydrography, direct velocity measurements and altimetric SSH consistently demonstrate the existence of mesoscale eddies in the area of study.

Even though the temporal and/or spatial coverage of some of the periods do not coincide, all of the measured parameters show the same qualitative behavior.

The region is strongly dominated by the formation of geostrophically balanced meanders and eddies. The region around Bahía Vizcaíno is characterized by the formation of anticyclonic eddies, seemingly due to the tendency of the California Current flow to follow the coast. Off Punta Eugenia however, the generated eddies tend to rotate cyclonically as the countercurrent along the coasts have a propensity to reverse its direction of flow. The observed circulation for this "transition region" was the same as that described by Roden (1971).

In spring, the maps of geostrophic circulation obtained from the hydrographic data show a meandering coastal flow without eddies, even though the winds are strongest during this season. The lack of eddies in spring could be associated with the more homogenous winds, as well as with the building up of coastal fronts that eventually become unstable and develop into eddies.

The generation of the eddies occurs mainly during the summer period while their propagation occurs during the summer, fall and winter seasons. As the Hovmüller altimetry plot does not show a clearly defined period in the generation of the eddies, this seems to suggest an instability process as the possible generation mechanism.

Finally, even though we do not specifically investigate the dynamics of the westward propagation of the eddies, it is worthwhile to point out that their speed of propagation is consistent with the theoretical propagation speed of a Rossby wave.

References

Aguirre-Hernández, E., Gaxiola-Castro, G., Najera-Martínez, S., Baumgartner, T., Kahru, M., Greg Mitchel, B. 2004. Phytoplankton absorption, photosynthetic parameters, and primary production off Baja California: summer and autumn 1998, Deep-Sea Research II 51, this issue [doi: 10.1016/dsr2.2004.05.015].

Auad, G., Parés-Sierra, A., Vallis, K.G., 1991. Circulation and energetic of a model of the California Current System. Journal of Physical Oceanography 21, 1334–1552.

Batteen, M.L., 1997. Wind-forced modeling studies of currents, meanders and eddies in the California Current System. Journal of Geophysical Research 102(C1), 985–1010.

Batteen, M.L., Haney, R.L., Tielking, T.A., Renaud, P.G., 1989. A numerical study of wind forcing of eddies and jets in the California Current System. Journal of Marine Research 47, 493–523.

Bretherton, F.P., Davis, R.E., Fandry, C.B., 1976. A technique for objective analysis and design of oceanographic experiments applied to MODE-73. Deep-Sea Research I 23, 559–582.

Candela, J., Beardsley, R.C., Limeburner, R., 1992. Separation of tidal and subtidal currents in ship-mounted acoustic Doppler current profiler observations. Journal of Geophysical Research 97, 769–788.

Chelton, D.B., 1982. Large-scale response of the California Current to forcing by the wind stress curl. CalCOFI Rep. Vol. 3, 130–184.

Chereskin, T.K., Trunnell, M., 1996. Correlation scales, objective mapping, and absolute geostrophic flow in the California Current. Journal of Geophysical Research 101, 22,619–22,629.

Chereskin, T.K., Levine, M.D., Harding, A.J., Regier, L.A., 1989. Observations of near-inertial waves in acoustic Doppler current profiler measurements made during MIL-DEX. Journal of Geophysical Research 94, 8135–8145.

Ducet, N., Le Traon, P.Y., 2000. Global high-resolution mapping of ocean circulation from TOPEX/Poseidon and ERS-1 and 2. Journal of Geophysical Research 105, 477–498.

Durazo, R., Baumgartner, T.R., 2002. Evolution of oceanographic conditions off Baja California: 1997–1999. Progress in Oceanography 54, 7–31.

Figueroa-González, J. C., 2002. Circulación superficial considerando geostrofía y la deriva de Ekman, entre Ensenada, B. C. y San Carlos, B. C. S., durante 1999. Bachelor Oceanography Thesis. FCM-UABC, 60pp.

Firing, E., Ranada J., Caldwell, P., 1995. Processing ADCP data with CODAS software system version 3.1, User's Manual.

García, C. J., Durazo, R. A., Baumgartner, T. M., Lavaniegos, E. R., 1999. Hidrografía en la zona sureña de la Corriente de California, Campaña IMECOCAL 9901. B/O Francisco de Ulloa. 14/01–31/01 de 1999. Informe Técnico. Departamento de Ecología, CICESE. 126pp.

Gill, A.E., 1982. Atmosphere-Ocean Dynamics. International Geophysics series 30, 421–428.

Haidvogel, D.B., Beckman, A., Hedstrom, K.S., 1991. Dynamic simulation of filament formation and evolution in the coastal transition zone. Journal of Geophysical Research 96, 15,017–15,040.

Halliwel, G., Williams, R.G., Viera, K., Mooers, C.N.K., 1983. Ocean currents. In: Godshall, F.A., Williams, R.G., (Eds.), A Climatology and Oceanographic Analysis of the California Pacific outer Continental shelf region. NOAA and US Department of the Interior AA551-IA9-2, 1182pp

Herrera, H., Parés-Sierra, A., 1994. Propagacion de variaciones de baja frecuencia en la temperatura superficial del Pacifico nor-oriental. Geofisica Internacional 33 (3), 469–486.

Hickey, B.M., 1979. The California Current System, hypotheses and facts. Progress in Oceanography, 191–279.

Ikeda, M., Emery, W.J., 1984. Satellite observations and modeling of meanders in the California Current system off Oregon and Northern California. Journal of Physical Oceanography 14, 1434–1450.

Ikeda, M., Emery, W.J., Mysak, L.A., 1984a. Seasonal variability in meanders of the California Current System off Vancouver Island. Journal of Geophysical Research 89, 3487–3505.

Ikeda, M., Mysak, L.A., Emery, W.J., 1984b. Observations and modelling of satellite-sensed meanders and eddies off Vancouver Island. Journal of Physical Oceanography 14, 3–21.

Le Traon, P.Y., Ogor, F., 1998. ERS 1-2 orbit improvement using TOPEX/Poseidon: The 2 cm challenge. Journal of Geophysical Research 103, 8045–8057.

Lynn, R.J., Simpson, J.J., 1987. The California Current System: The seasonal variability of its physical characteristics. Journal of Geophysical Research 92, 12,947–12,966.

Madsen, O.S., 1977. A realistic model of wind-induced Ekman boundary layer. Journal of Physical Oceanography 7, 248–255.

McCreary, J., Fukamachi, Y., Lu, P., 1992. A non-linear mechanism for maintaining coastally trapped eastern boundary currents. Journal of Geophysical Research 97, 5677–5692.

Parés-Sierra, A., O'Brien, J.J., 1989. The seasonal and interannual variability of the California Current System: A numerical model. Journal of Geophysical Research 94, 3159–3180.

Parés-Sierra, A., White, W.B., Tai, C.K., 1993. Wind-driven coastal generation of annual mesoscale eddy activity in the California Current System: A numerical model. Journal of Geophysical Research 23, 1110–1121.

Pond, S., Pickard, G.L., 1978. Introductory Dynamic Oceanography. Pergamon Press, Oxford, p. 241.

Roden, G.I., 1971. Aspects of the transition zone in the northeastern Pacific. Journal of Geophysical Research 76, 3462–3475.

Strub, P.T., James, C., 2000. Altimeter-derived variability of surface velocities in the California Current System: 2 Seasonal circulation and eddy statistics. Deep-Sea Research II 47, 831–870.

Strub, P.T., Kosro, P.M., Huyer, A., CTZ Collaborators, 1991. The nature of the cold filaments in the California Current System. Journal of Geophysical Research 96, 14,743–14,768.

Walstad, L.J., Allen, J.S., Kosro, P.M., Huyer, A., 1991. Dynamics of the coastal transition zone through data assimilation studies. Journal of Geophysical Research 96, 14,959–14,977.

White, W.B., Saur, J.F.T., 1983. A sorce of interannual baroclinic waves in the eastern subtropical North Pacific. Journal of Physical Oceanography 13, 531–544.